

PAPER

Preparation and characterization of a supported system of $\text{Ni}_2\text{P}/\text{Ni}_{12}\text{P}_5$ nanoparticles and their use as the active phase in chemoselective hydrogenation of acetophenone

To cite this article: Dolly C Costa *et al* 2018 *Nanotechnology* **29** 215702

View the [article online](#) for updates and enhancements.

Related content

- [Effects of surface activation on the structural and catalytic properties of ruthenium nanoparticles supported on mesoporous silica](#)
Xianfeng Ma, Rui Lin, Christopher Beuerle et al.
- [A novel synthetic route to freely adjust the crystal structures of Ni-P compounds](#)
Hanghui Xu, Shaoxiang Lu and Lili Ren
- [Synthesis, characterization and properties of hollow nickel phosphide nanospheres](#)
Yonghong Ni, Ali Tao, Guangzhi Hu et al.



IOP | ebooks™

Bringing you innovative digital publishing with leading voices to create your essential collection of books in STEM research.

Start exploring the collection - download the first chapter of every title for free.

Preparation and characterization of a supported system of $\text{Ni}_2\text{P}/\text{Ni}_{12}\text{P}_5$ nanoparticles and their use as the active phase in chemoselective hydrogenation of acetophenone

Dolly C Costa¹, Analía L Soldati², Gina Pecchi³, José Fernando Bengoa¹, Sergio Gustavo Marchetti¹ and Virginia Vetere¹ 

¹ Centro de Investigación y Desarrollo en Ciencias Aplicadas 'Dr Jorge J. Ronco'-CINDECA (UNLP-CONICET-CICBA). Calle 47 N° 257, (1900) La Plata, Bs. As. Argentina

² Grupo de Caracterización de Materiales, Centro Atómico Bariloche, CONICET. Av. Bustillo 9500, San Carlos de Bariloche, Río Negro, Argentina

³ Departamento de Físico Química, Facultad de Ciencias Químicas, Universidad de Concepción. Casilla 160-C, Concepción, Chile

E-mail: vetere@quimica.unlp.edu.ar

Received 28 December 2017, revised 23 February 2018

Accepted for publication 2 March 2018

Published 26 March 2018



Abstract

$\text{Ni}_2\text{P}/\text{Ni}_{12}\text{P}_5$ nanoparticles were obtained by thermal decomposition of nickel organometallic salt at low temperature. The use of different characterization techniques allowed us to determine that this process produced a mixture of two nickel phosphide phases: Ni_2P and Ni_{12}P_5 . These nickel phosphides nanoparticles, supported on mesoporous silica, showed activity and high selectivity for producing the hydrogenation of the acetophenone carbonyl group to obtain 1-phenylethanol. This is a first report that demonstrates the ability of supported $\text{Ni}_2\text{P}/\text{Ni}_{12}\text{P}_5$ nanoparticles to produce the chemoselective hydrogenation of acetophenone. We attribute these special catalytic properties to the particular geometry of the Ni–P sites on the surface of the nanoparticles. This is an interesting result because the nickel phosphides have a wide composition range (from Ni_3P to NiP_3), with different crystallographic structures, therefore we think that different phases could be active and selective to hydrogenate many important molecules with more than one functional group.

Keywords: monodisperse nanoparticles of nickel phosphides, Ni_2P , Ni_{12}P_5 , hydrogenation, chemoselectivity, acetophenone

(Some figures may appear in colour only in the online journal)

1. Introduction

Over the last few decades a new family of hydrotreating catalysts, the transition metal phosphides, has emerged. They have been widely used in hydrodesulfurization (HDS) and hydrodenitrogenation (HDN) processes [1, 2]. The Oyama group have worked in this area in particular [3–6]. These phosphides have physical properties, which are similar to

those of ordinary metallic compounds: they are hard and strong, are good heat and electricity conductors, and have high thermal and chemical stability.

Among the various transition metal phosphides, nickel phosphide is the most active catalyst for HDS and HDN reactions [7–9]. Since 1990 a temperature-programmed reduction method has been developed as a simple and economical way to prepare metal phosphides [10]. However, the

main disadvantage of this method is the high reduction temperature required due to the great stability of the P–O bond. These conditions lead to a wide distribution of sizes of the nickel phosphide particles [11, 12].

More recently, nickel phosphides nanoparticles (NPs) have been obtained by thermal decomposition of nickel organometallic salts in the presence of a reducing agent and alkyl, or phenyl phosphines as a phosphorus source [12–15]. It is well known that up to 850 °C there are many stable phases of nickel phosphides with compositions between Ni_3P and NiP_3 . However, Ni_2P is obtained in most of the cases in the NP range. Another composition that frequently appears is Ni_{12}P_5 . This versatility in the arrangements allows the production of active sites with very different geometric characteristics, changing the electronic density of the Ni atoms. Thus, the selectivity of the catalytic reaction could be drastically changed.

As already mentioned, the excellent catalytic properties of nickel phosphides for HDS and HDN probably indicate that they have good activity in hydrogen transfer reactions, such as hydrogenation. Additionally, the particular geometric characteristics of the active sites could produce the chemoselective hydrogenation of double bonds in those molecules with more than one functional group. Previous research on this behavior, with nickel phosphides catalysts, is scarce. Wang *et al* studied the chemoselective hydrogenation of cinnamaldehyde with nickel phosphides catalysts supported on SiO_2 [16]. They prepared these catalysts by temperature-programmed reduction of nickelphosphates. These catalysts showed high selectivity in the hydrogenation of this unsaturated aldehyde to the saturated one. Thus, they obtained great production of hydrocinnamaldehyde from hydrogenation of cinnamaldehyde. However, it is well known that in the hydrogenation of α,β -unsaturated aldehydes thermodynamics favors the hydrogenation of an aliphatic C=C bond over the C=O group in around 35 kJ mol^{-1} , and due to kinetic reasons the reactivity of the C=C bond is higher than that of C=O [17]. Therefore, the article of Wang *et al* shows the hydrogenating capacity of Ni_2P and Ni_{12}P_5 , but without chemoselectivity.

On the other hand, there is a higher challenge related to aromatic alcohols if these have to be obtained from a selective hydrogenation of aromatic ketones. These types of alcohols are widely used in the production of drugs and in fine chemicals. The aromatic ketone molecules have two groups that can be hydrogenated. Therefore, great effort has been performed to achieve these chemoselective hydrogenations. When Pt, Rh and Ru catalysts are used, they exhibit comparable reactivity towards the hydrogenation of the carbonyl group and the aromatic ring [18–24]. In order to enhance the selectivity of C=O hydrogenation a suitable support, or modifications by the use of additives on these metals, is needed. On the other hand, Pd supported catalysts are highly reactive for the C=O hydrogenation towards C–OH, but then they catalyze the hydrogenolysis of C–OH to give ethylbenzene as a final product [25–28].

Considering these difficulties, we guess that the expected results could be obtained using a compound with metallic

characteristics with moderate hydrogenation capacity and catalytic sites with particular geometries. Thus, the spatial configuration of the adsorbed molecules and the structural characteristics of the catalytic sites would allow ‘tuning’ of the proper arrangement to reach the appropriate hydrogenation. These characteristics could be present in nickel phosphides because they have metallic properties that are able to produce moderate hydrogenations due to the diluting effect of the phosphorus atoms. In addition, the wide range of stoichiometric compositions, with very different crystallographic structures, produces surface sites with very diverse geometries. Therefore, there could be catalytic sites, with particular geometries that could hydrogenate different aromatic ketones to the desired product. Following these ideas, the aim of the present work is to explore the possibility to obtain a chemoselective hydrogenation of acetophenone to produce 1-phenylethanol using nickel phosphide species as catalyst. To our knowledge, this is the first report on this application up to now.

In addition, in order to avoid possible effects of the NP sizes on the reaction selectivity, we pre-synthesized NPs of nickel phosphides monodisperse, which were then supported on mesoporous silica and used as catalyst in the acetophenone hydrogenation in liquid phase.

2. Experimental

2.1. Nanoparticle synthesis

In a one-pot synthesis, determined amounts of nickel(II) acetylacetonate ($\text{Ni}(\text{acac})_2$, 1 mmol), oleylamine as solvent and reductant (OA, 10 mmol), and triphenylphosphine as ligand and phosphorus source (PPh_3 , 0.8 mmol) were directly added into a three-neck round bottom flask fitted with a condenser and magnetic stirring. The two remaining necks were used to introduce a thermocouple with a glass sheath and a flow of Ar. The mixture was heated at 220 °C for two hours. Finally, the NPs were purified and isolated, precipitating the suspension with acetone and re-dispersed in n-hexane.

The NPs were characterized by x-ray diffraction (XRD), diffuse light scattering (DLS), transmission electron microscopy (TEM), selected area electron diffraction (SAED), Fourier transformer infrared spectroscopy (FT-IR) and magnetization versus applied field (M versus H). In addition, the Ni content in the suspension and in the catalyst was determined by atomic absorption spectroscopy (AA).

2.2. Support synthesis

The mesoporous silica, used as support, was synthesized following the method proposed by Ishihara *et al* [29]. An acid-base-catalyzed sol–gel process with a gel skeletal reinforcement was adopted. Briefly, tetraethyl orthosilicate (TEOS) was used as silica source. This compound was dissolved in 2-propanol and HCl at 25 °C. The pH of the mixture was adjusted to 5 by adding aqueous NH_3 solution and the

gelation process was performed at 50 °C over 5 h. This gel was then introduced into deionized water at 50 °C for 24 h. After this treatment, the gel was thoroughly washed with 2-propanol to remove the water present into the pores. After this step, the gel was contacted with 80% TEOS/20% 2-propanol solution at 50 °C for 48 h. Finally, the gel was washed with 2-propanol to remove the remaining 80% TEOS/20% 2-propanol solution, dried and finally calcined at 600 °C for 3 h in air flow.

The final solid was characterized by N₂ adsorption at −196 °C and TEM.

2.3. Catalyst preparation

The catalyst was prepared by wetness impregnation of the mesoporous silica with the NP suspension with the aim of obtaining a nominal Ni loading of 5% wt/wt.

In order to eliminate the surfactant (PPh₃) from the surface of the NPs two different treatments were performed. The first one was a thermal treatment at 400 °C in Ar flow (60 cm³ min^{−1}) over 24 h, and the second one consisted of several washings with CHCl₃. The catalyst was characterized by thermal gravimetric analysis and differential thermal analysis (TGA-DTA), TEM and scanning electron microscopy (SEM).

2.4. Characterizations

XRD patterns were recorded using a standard automated powder XRD system Philips PW1710 with a diffracted-beam graphite monochromator, using Cu K_α radiation ($\lambda = 1.5406 \text{ \AA}$) in the range $2\theta = 35^\circ$ – 60° with steps of 0.05° and counting time of 6 s/step.

In the DLS measurements, the time correlation function $G(q, t)$ of the light scattering intensity was measured at the scattering angle $\theta = 90^\circ$ with a goniometer ALV/CGS-5022F with multiple tau digital correlator ALV-5000/EPP covering a 10^{-6} – 10^3 s time range. The light source was a helium/neon laser ($\lambda = 632.8 \text{ nm}$) operating at 22 mW. All of the measurements were carried out at room temperature. In order to obtain appropriate estimations of the size of the particles, number and weight, average hydrodynamic radii were calculated from the time correlation function with the package CONTIN [30].

For TEM measurements two different pieces of equipment were used. Samples for analysis were prepared by drying a dispersion of the NPs on amorphous carbon coated copper grids. TEM micrographs were obtained on a JEOL model JEM-1200 EX II microscope and on a Philips CM 200 UT TEM and high resolution TEM equipped with an ultra-twin objective lens. The electron source used was a LaB6 filament operated at 200 keV. The nominal resolution was 0.2 nm for the high resolution mode. The microscope was equipped with a CCD camera for digital acquisition; contrast and illumination were linearly adjusted after using commercially available image treatment programs. Point elemental analysis was done using an EDS (EDAX) system coupled to the TEM. The excited spot was of 150 nm diameter on the

surface of the sample and the acquisition time was 100 s. In addition, an SAED was obtained.

The TGA-DTA measurements were performed on a RIGAKU Thermo plus EVO equipment. The samples were located inside an alumina crucible and heated from room temperature up to 1000 °C at a heating rate of $10^\circ\text{C min}^{-1}$ under air flow ($100 \text{ cm}^3 \text{ min}^{-1}$).

A FT-IR Jasco spectrometer model 4200 equipped with a PIKE diffuse reflectance IR cell with a resolution of 1 cm^{-1} was used. From 200 to 400 scans were accumulated in each case.

The magnetic measurements were carried out using a multipurpose physical magnetic system (MPMS) superconducting quantum interference device (SQUID) from Quantum Design. The M versus H curve was recorded at 6 K up to a maximum magnetic field of 5 T.

The textural properties, specific surface area (S_g), specific pore volume (V_p) and pore diameter (D_p), were measured with a Micromeritics ASAP 2020 V1.02 E device.

The SEM measurements were performed with an SEM model FEI ESEM Quanta 200. The Ni/P ratio on the catalyst surface was determined by energy dispersive analysis of x-ray with an EDAX SDD Apollo 40 probe.

2.5. Catalytic tests

Hydrogenation of acetophenone was carried out in a stirred autoclave reactor at a pressure of H₂ of 1 MPa and a temperature of 80 °C, using 0.25 g catalyst and n-heptane as solvent. The experimental conditions for the catalytic tests were specifically chosen to avoid mass transfer control. The course of the reaction was followed by gas chromatography in a GC Varian 3400 chromatograph equipped with a capillary column of 30 m CP wax 52 CB and FID. The identification of the diverse reaction products was accomplished by GC/MS using Shimadzu QP5050 equipment.

3. Results and discussion

In figure 1, the XRD pattern of the as-synthesized NPs is shown. The detected peaks at around $2\theta = 40.5^\circ$, 44.2° , 46.8° and 54.0° could be assigned to Ni₁₂P₅ (tetragonal, PDF 74-1381) or Ni₂P (hexagonal, PDF 74-1385) respectively. In addition, the peaks at about 38.4° and 48.8° appear exclusively in Ni₁₂P₅. The crystalline planes assignable to Ni₁₂P₅ are indicated in red and those corresponding to Ni₂P in blue. After analyzing some aspects of the diffractogram we can observe that:

- the signal at 48.8° appears exclusively in Ni₁₂P₅ and represents its most intense peak,
- both phosphides show a peak at around 40.5° , which corresponds to the most intense signal of the Ni₂P. However, for Ni₁₂P₅ it represents approximately 16% of its most intense peak.

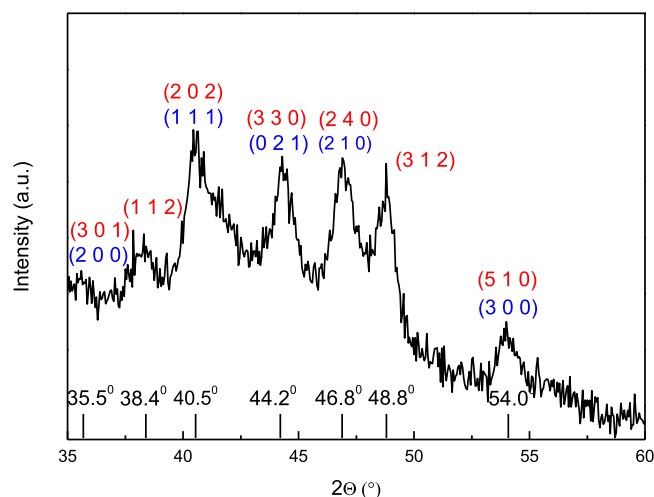


Figure 1. XRD diagram of nickel phosphides NPs. Red numbers correspond to diffraction planes of Ni_{12}P_5 and blue numbers to Ni_2P .

Considering that the peaks at 40.5° and 48.8° have similar intensities, we can conclude that a mixture of both phosphides was obtained. All peaks are considerably broadened due to the small size of the NPs (this topic will be described below). Consequently, the precise assignment of the 2θ values is not possible in some of them. For the same reason, the peaks at $2\theta = 44.6^\circ$ and 41.6° assignable to the planes (0 2 1) of Ni_2P and (3 3 0) of the Ni_{12}P_5 , respectively, cannot be distinguished. Finally, it is worth noting that the quality of the diffractogram is not optimal because to deposit a good quantity of the NPs on the XRD holder, in order to reach a homogeneous covering, is a hard task.

In order to obtain the size distribution of the NPs we performed DLS measurements. It is worth mentioning that DLS measurements are easy and fast to perform and also provide significant statistical information. As a disadvantage, the values obtained are the hydrodynamic diameters, that is, the sum of the NP diameter plus the thickness of the NP coverage. Depending on the system a significant or a negligible difference compared to the real diameter can be found [31]. The results obtained by this technique show that the NP suspension is monodisperse (polydispersity index <0.1) and they have an average diameter between 12 and 14 nm. In order to confirm this average diameter we obtained TEM micrographs. In figure 2 can be seen two representative micrographs. Figure 3 shows the histogram obtained counting 622 NPs. The histogram was fitted using a log-normal distribution according to previous studies showing that very small particles (i.e. lower than 20 nm) present a log-normal size distribution [32]. The statistical parameters obtained from the fitting produced an average diameter of 9.6 ± 0.2 nm. Considering the DLS results the NPs are monodisperse and the average diameter value is very similar to that obtained by TEM, although slightly lower in coincidence with the previous explanation.

To obtain structural information of the NPs, the SAED was acquired and analyzed. Table 1, shows the lattice spacing measured from the rings of the diffraction pattern (figure 4) and compares them with the known lattice spacing for bulk

Ni_{12}P_5 and Ni_2P . This technique indicates the presence of a mixture of both phosphides, but in a less categorical way because, in the analyzed spot, the diffraction rings corresponding to the (1 1 2) and (3 1 2) crystallographic planes of Ni_{12}P_5 were not detected.

On the other hand, the lattice spacing was obtained using the inverse Fourier transform of high resolution TEM images of three different and isolated NPs (figures 5(A)–(C)). These values were: 2.03 Å, 2.21 Å, 2.50 Å and 2.34 Å. The first three values could be assigned to the (0 2 1), (1 1 1) and (2 0 0) planes of Ni_2P or the (3 3 0), (2 0 2) and (3 0 1) planes of Ni_{12}P_5 respectively, and the spacing of 2.34 Å corresponds exclusively to the (1 1 2) plane of Ni_{12}P_5 . It can be seen that only one class of crystalline planes is present in each of the NPs; there are no planes changing their direction and all planes are straight. Therefore, each NPs has only one nickel phosphide phase. In summary, the suspension would consist of a mixture of pure NPs of Ni_{12}P_5 and Ni_2P .

The magnetic characterization was performed on the NP suspension. The M versus H loop obtained at 6 K is shown in figure 6. This curve can be fitted with a Brillouin function denoting paramagnetic behavior. This result is coherent with the presence of Ni_2P or Ni_{12}P_5 [33–36]. It is important to remark that a superparamagnetic behavior can be discarded taking into account that the temperature at which the measurement was done. This conclusion can be obtained considering that metallic nickel NPs smaller than 15 nm are typically superparamagnetic at room temperature, but they are magnetically blocked at 10 K [37]. As the magnetic anisotropy constant of nickel phosphides is about six times higher than the one of the metallic nickel, their magnetic blocking temperature must be considerably higher than 6 K.

On the other hand, the Ni/P ratio obtained from the average of several EDAX measurements on the calcined catalyst was 2.35. Taking into account that the stoichiometric ratios are 2.4 for Ni_{12}P_5 and 2 for Ni_2P , a combination of the presence of both phases could explain this experimental result with Ni_{12}P_5 as a dominant phase. Using the expression: $(\text{Ni}/\text{P})_{\text{exp}} = 2X + 2.4Y$, where X = molar fraction of Ni_2P and Y = molar fraction of Ni_{12}P_5 and considering that $X + Y = 1$, the following composition of the mixture can be obtained: 87% molar of Ni_{12}P_5 and 13% molar of Ni_2P . It is necessary to highlight that EDAX analysis attached to SEM is not fully reliable for obtaining quantitative values. However, this technique can be used to obtain a rough estimation of the molar percentage of the nickel phosphide species. In addition, this assay reinforces the conclusion about the presence of both phases of nickel phosphides. It is interesting to mention that, in the catalyst without calcination, the Ni/P ratio determined by this technique was 0.80. This result can be explained because the presence of Ph_3P on the NPs surface increases the P content.

There is a controversy about the synthesis temperature necessary to obtain nickel phosphide from organophosphorus compounds. In this way, the research groups led by Sanchez and Brock (probably the groups that have studied this subject more in depth) consider that temperatures higher than 330°C are required [36, 38, 39]. Other authors have used the same

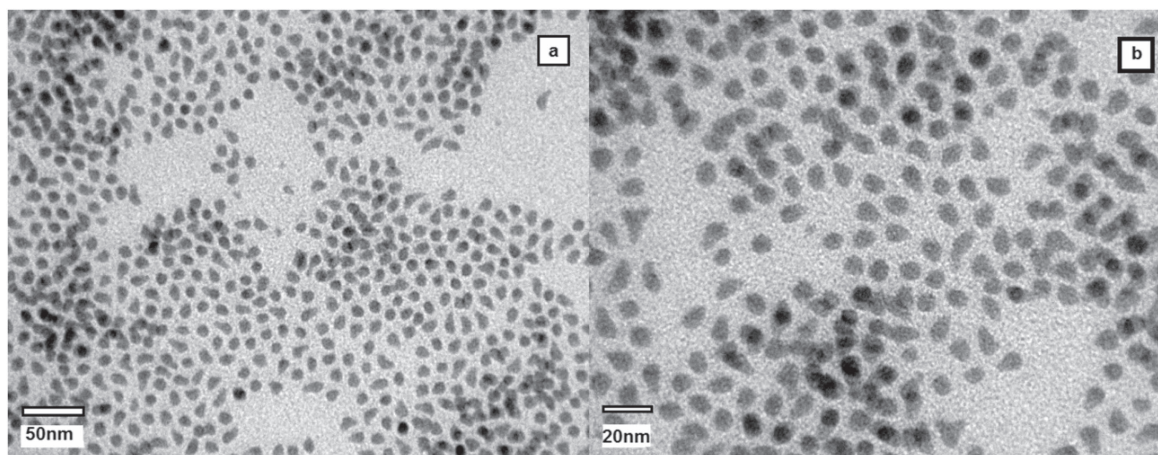


Figure 2. (a) and (b) representative TEM images of nickel phosphide NPs.

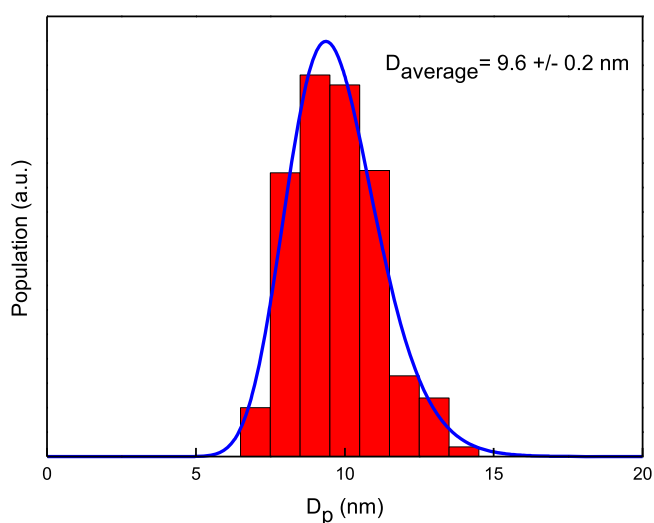


Figure 3. Histogram of the sizes of nickel phosphide NPs obtained from TEM. The blue line was obtained by fitting the results assuming a log-normal distribution.

Table 1. Comparison of lattice spacing between the nickel phosphide NPs, measured using the SAED technique, with the powder diffraction file data.

Experimental d -spacing (\AA) obtained from SAED	d -spacing (\AA) from data files	
	Ni_2P	Ni_{12}P_5
2.27	2.21	2.19
2.00	2.03	2.04
1.76	1.69	1.70

temperature [12, 40, 41]. However, Wang *et al* suggested that this decomposition can start at 240 °C [41]. Subsequently, it was confirmed that at 200 °C–230 °C, an amorphous Ni_xP_y is produced. In addition, crystalline Ni_2P can be obtained maintaining this temperature over 24 h [42, 43]. It is important to remark that, in these studies, the phosphorus compound used is trioctylphosphine instead of triphenylphosphine. On the other hand, it is

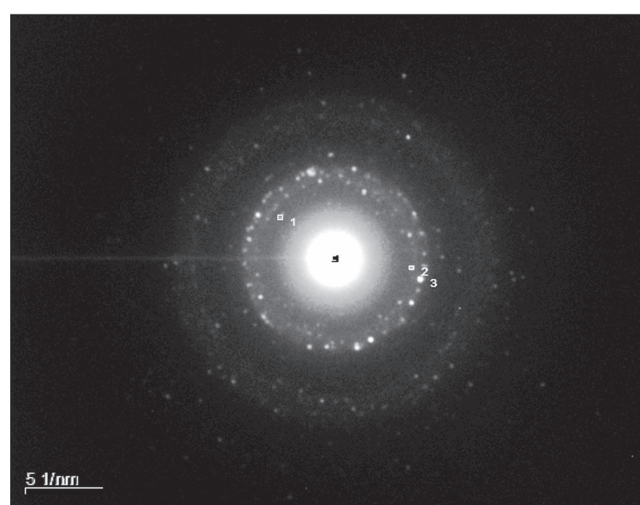


Figure 4. d -spacing of the nickel phosphide NPs determined by SAED.

commonly accepted that the small nickel nuclei act as a catalyst to break the P-organic ligand bond. Then, this free P diffuses inside the nickel NPs and produces nickel phosphide. We think that the different phosphorus compound used and the quantity of nickel nuclei produced in the initial step (as a consequence of the nickel(II) acetylacetonate : oleylamine ratio) would explain the obtained results.

To determine if the OA and PPh_3 remain on the NPs surface, we obtained the FT-IR spectrum (figure 7). It was acquired by mechanical mixing of the NP suspension with KBr and subsequent drying. We chose this procedure, instead of using the supported system, because SiO_2 support has bands that overlap with the ones belonging to OA and PPh_3 . The bands indicated by red arrows can be assigned to OA. Thus, the bands at 2927 and 2854 cm^{-1} correspond to stretching C–H of methyl and methylene groups respectively, at 1710 cm^{-1} to C=O stretching (the carbonyl group is produced by reaction between OA and acetylacetonate groups) and at 1580 cm^{-1} to aliphatic C=C [38, 44, 45]. On the other hand, the bands pointed out by green arrows indicate the presence of PPh_3 . The weak signal at 3000 cm^{-1} is assigned to stretching of the C–H bond and at

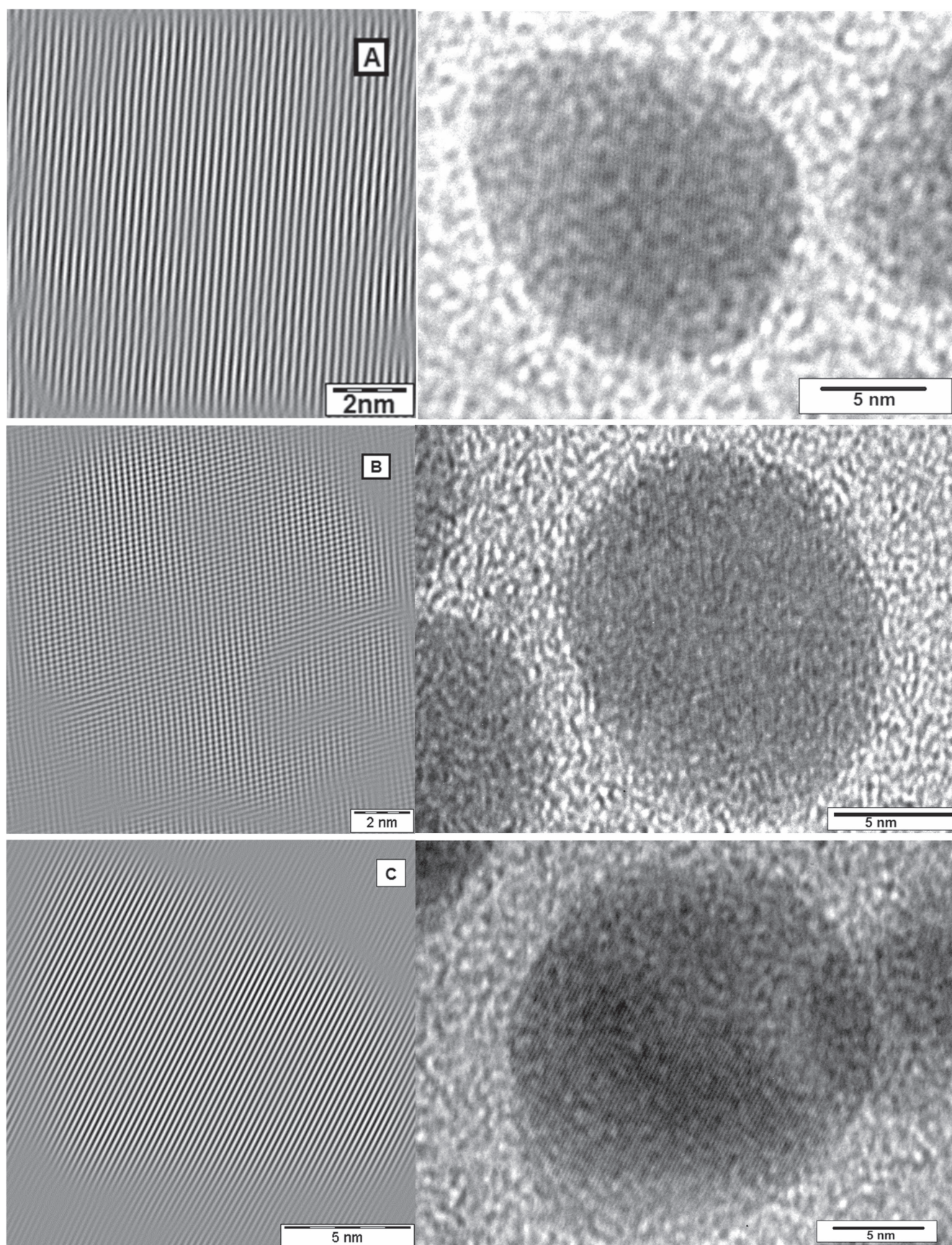


Figure 5. (A), (B) and (C) High resolution TEM of three different isolated NPs (right) and their inverse Fourier transforms (left).

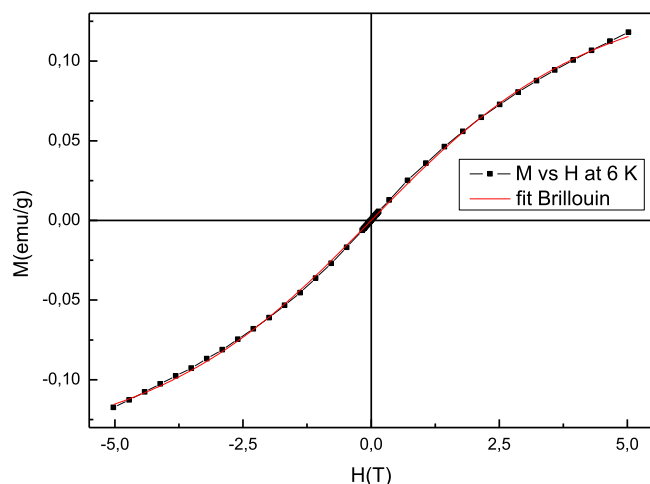


Figure 6. Hysteresis cycle of nickel phosphide nanoparticles at 6 K using a maximum applied magnetic field of $H = 5$ T.

1655 cm^{-1} to aromatic C=C. In addition, the bands at 1454 and 1421 cm^{-1} correspond to the stretching of the bond P-C₆H₅. Finally, the bands at 1065 and 960 cm^{-1} are attributed to aromatic C-H in-plane vibrations and at 742 and 720 cm^{-1} to out-of-plane vibrations [38, 45, 46]. The characteristic bands appear slightly shifted, indicating that the hydrocarbon chains in the monolayer surrounding the NPs are close packed [47]. The presence of these surfactants on the NP surface would explain the diameter differences between DLS and TEM results. Finally, the blue arrow at 1080 cm^{-1} can be assigned to the stretching of the metallic Ni atom bound to P=O. This species would be originated by the oxidation of the PPh₃ on the surface of the NPs when they are contacted with air during the FT-IR spectrum measurement. Considering that the spontaneous oxidation of PPh₃ by O₂, either in the solid state or in solution, is very slow in air contact, the nickel phosphide surface would act as a catalyst in this process [38]. The coverage of the NP surface by OA and PPh₃ would block the catalytic active sites. This has been confirmed based on the fact that the catalytic reaction, using the catalyst as it was prepared (without any post-synthesis treatment), was found inactive.

The silica support is made up of nanometric spheres of about 200 nm with interparticular channels (figure 8). Their textural properties are: BET specific surface area: $508\text{ m}^2\text{ g}^{-1}$, average pore diameter, obtained by the BJH method: 27 nm and pore volume: $2.5\text{ cm}^3\text{ g}^{-1}$. The Ni loading of the catalyst, determined by AA, was of 5% wt/wt.

After wetness impregnation of the silica support with the NP nickel phosphides suspension, TEM micrographs show that the NPs did not change their size and they are located preferentially on the surface of the SiO₂ spheres, but some of them are placed inside the interparticular mesoporous (figure 8).

With the purpose of studying the elimination of the NP superficial covering, a TGA-DTA measurement was performed. Figure 9 shows that the highest velocity of mass loss

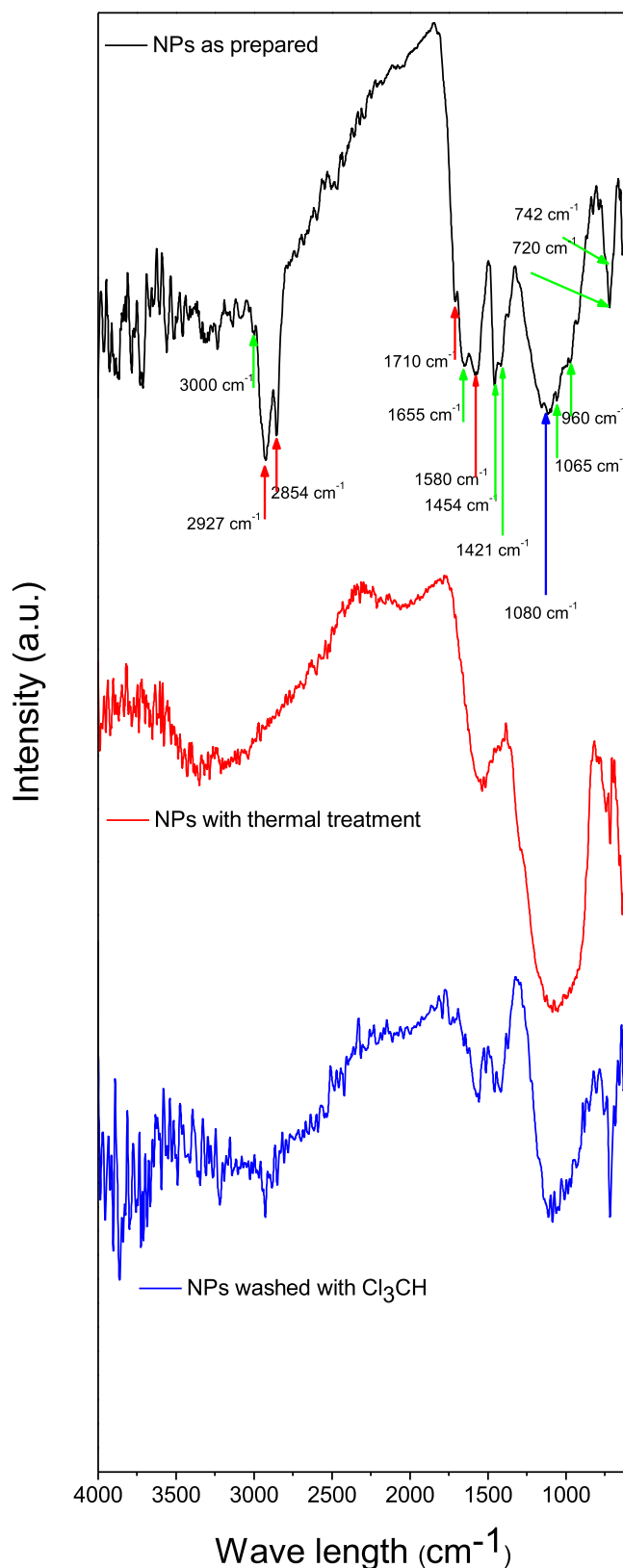


Figure 7. FT-IR of nickel phosphide NPs as prepared (black spectrum), NPs with thermal treatment (red spectrum) and NPs washed with Cl₃CH (blue spectrum).

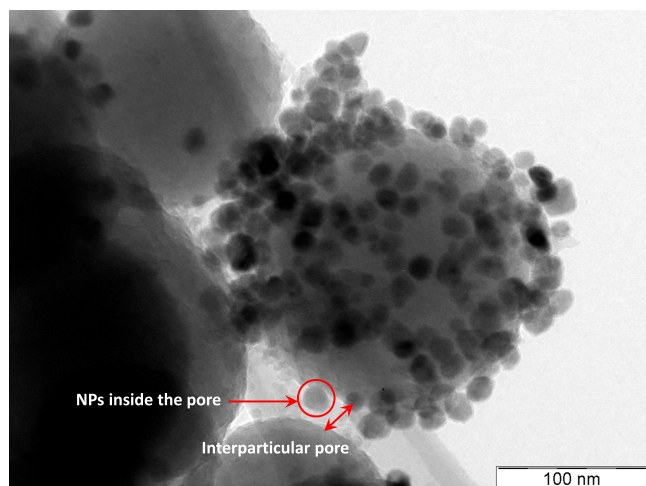


Figure 8. TEM image of nickel phosphide NPs supported on mesoporous silica.

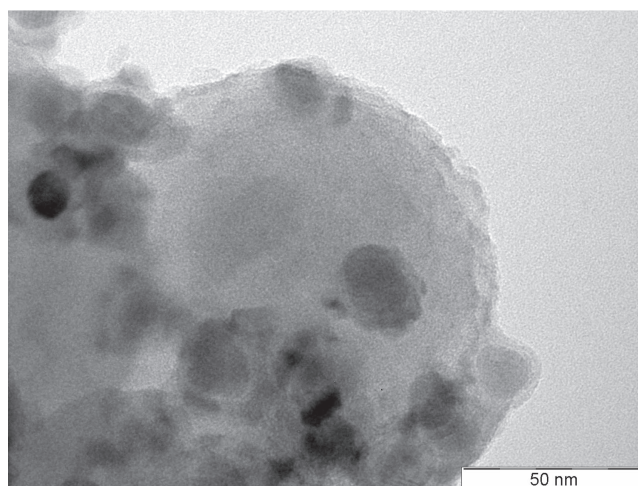


Figure 10. TEM image of nickel phosphide NPs supported on mesoporous silica after thermal treatment.

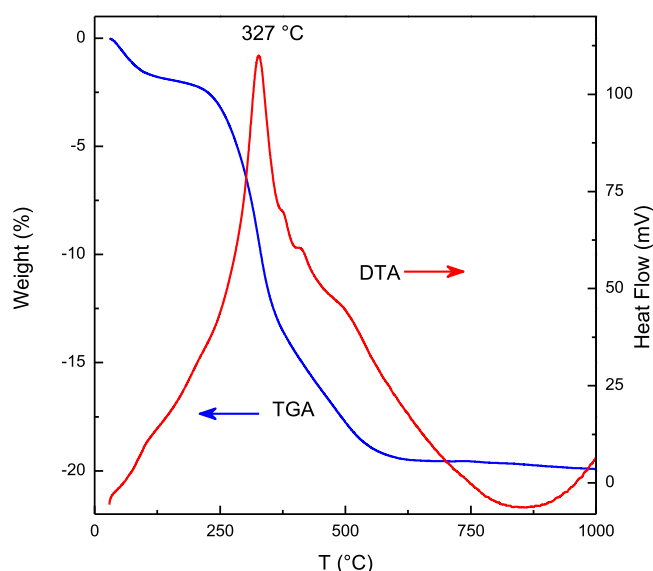


Figure 9. TGA-DTA diagrams of nickel phosphide NPs.

(attributed to the surfactant elimination) occurs at about 330 °C. Taking into account that the nickel phosphides are stable up to 890 °C, the catalyst was heated at 400 °C in Ar flow over 24 h in order to eliminate the surfactant before performing the catalytic test [39]. Figure 10 shows a TEM micrograph that reveals that NP sintering did not occur during this treatment. This result is coherent with the high Tamman temperature of the nickel phosphide (about 560 °C). Above this temperature the mobility and reactivity of the atoms becomes appreciable and sintering could occur.

Figure 7 displays the NP FT-IR spectrum after this thermal treatment. Again, the spectrum was obtained by mechanical mixing of the NP suspension with KBr and this solid was then heated following the thermal treatment previously described. Figure 7 shows that all peaks assigned to OA have disappeared (bands at 2927, 2854, 1710 and 1580 cm^{-1}). Another interesting point is that the PPh_3 partially disappears. Thus, in the range of 720–740 cm^{-1} , the

bands attributed to aromatic C–H out-of-plane vibrations are clearly visible. On the other hand, the fine structure of the peaks at 1655, 1454 and 1421 cm^{-1} is lost and only a broad peak can be seen. According to the TGA-DTA results, the thermal treatment would be enough to eliminate the surfactants. A greater sensitivity of the FT-IR to detect surface species, in comparison with TGA-DTA technique, would explain this result. Therefore, we can infer that there are different types of surface sites able to adsorb the PPh_3 with different strength. This would be the result of the complex surface geometric structure of the nickel phosphides, as will be discussed below, and maybe these blocked sites could produce a decrease in the catalytic activity.

The main products of acetophenone hydrogenation are shown in scheme 1. If the carbonyl group is hydrogenated, 1-phenylethanol (PE) is obtained. On the other hand, the hydrogenation of the aromatic ring leads to cyclohexylmethylketone (CMK). The hydrogenation of both products can continue and 1-cyclohexylethanol (CE) can be obtained. In addition, traces of ethylbenzene (EB) and ethylcyclohexane (EC) can be produced. These products can be obtained by hydrogenolysis of C–O bond of intermediate alcohols or initial hydrogenation of C=O followed by dehydration and subsequent addition of hydrogen to C=C bond formed. Our objective is to produce a chemoselective hydrogenation of the carbonyl group to obtain 1-phenylethanol. Figure 11 shows that after 7 h of reaction time a conversion of 30% was obtained and the selectivity to 1-phenylethanol was of 90%. Therefore, the $\text{Ni}_2\text{P-Ni}_{12}\text{P}_5/\text{SiO}_2$ system is active in the acetophenone hydrogenation, and it has a high chemoselectivity to the desired product.

With the aim of finding an alternative method to eliminate the surface covering of the NPs, several washes of the supported catalysts with CHCl_3 were performed, following the method proposed by Senevirathne *et al* for a similar system (bulk Ni_2P unsupported) [12]. The FT-IR spectrum (figure 7) is very similar to the one after the thermal treatment of the sample. In agreement with this result, the activity and selectivity achieved after this treatment are very similar to

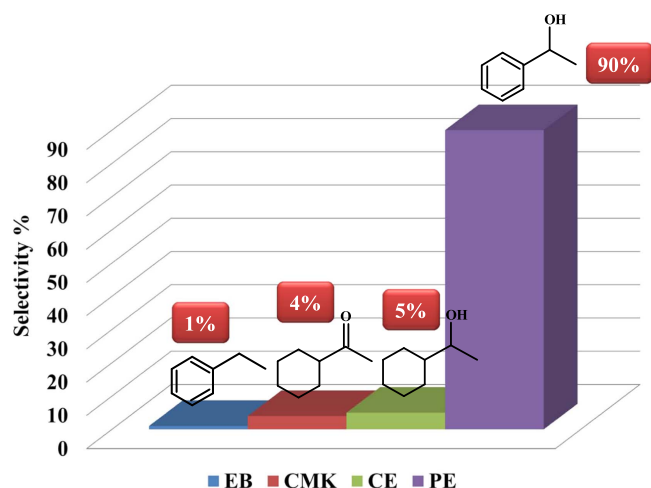


Figure 11. Selectivity diagram of acetophenone hydrogenation (operation conditions: (353 K, 1 MPa H_2 , 0.25 g catalyst).

Table 2. Conversion and selectivity to PE after 7 h of reaction for different treatments.

Treatment	Conversion (%)	$S_{1\text{-phenylethanol}}$ (%)
As prepared	0	—
Calcination in Ar	28	90
Washing with $CHCl_3$	30	92

those obtained with the thermal treatment (table 2). The advantage of the washing method is that it significantly reduces the surfactant elimination time. In addition, the EDAX analysis did not detect the presence of chloride ions. This is an important result because these ions can poison the active sites.

In order to analyze the chemoselective results of these nickel phosphide NPs, we will begin describing the explanation suggested by Chen *et al* for acetophenone hydrogenation on Pt/SiO₂ catalysts [48]. These authors proposed that the acetophenone has two preferential adsorption modes: $\eta^1(O)$ and $\eta^2(C,O)$ on the Pt surface. In the first mode, the molecule is coordinated to the catalyst surface by the oxygen atom of the carbonyl group and the aromatic ring remains parallel to the surface. Under these conditions, both the carbonyl group and the aromatic ring could be hydrogenated. In the second mode, the carbonyl group is coordinated through its π electrons (bridge coordination) and the aromatic ring is tilted with respect to the surface. This configuration would produce mainly 1-phenylethanol and the aromatic ring would not be hydrogenated. When nickel phosphides are used as a catalyst to hydrogenate acetophenone some important differences with pure metals must be considered. Thus, in these phases, P atoms have higher electronegativity than Ni atoms. As a consequence these atoms can be represented as $P^{\delta-}$ and $Ni^{\delta+}$, respectively. The $Ni^{\delta+}$ surface atoms behave as Lewis acid sites, attracting the atoms with negative charge density of the acetophenone, and at the same time, as metallic sites for hydrogenation [49]. However, this is not the only difference in comparison with pure transition metals because Sawhill

et al found that $C=O$ is adsorbed on Ni catalysts with two different geometries: linear and bridge-like. Instead, when $Ni_{12}P_5$ and Ni_2P were studied, the bridge adsorption disappeared and only the linear geometry remained [50]. The different adsorption modes of CO between Ni and $Ni_{12}P_5$ and Ni_2P cannot be justified by differences between the interatomic distances of the metallic centers. Thus, interatomic distance Ni–Ni, in metallic Ni, is 2.49 Å, while in $Ni_{12}P_5$ and in Ni_2P these distances are around 2.45 Å and 2.61 Å, respectively [51]. Therefore, these different adsorption modes could be attributed to a particular spatial arrangement of the nickel phosphide surfaces. Considering that, the electronic similarities between the carbonyl group and carbon monoxide, at a first approximation we could think that on $Ni_{12}P_5$ and Ni_2P , the acetophenone preferential adsorption mode would be $\eta^1(O)$. However, a $\eta^1(O)$ adsorption mode would favor the aromatic ring hydrogenation but our experimental results determined the opposite. We attributed this fact to the special configuration of the catalytic sites on the surface of the nickel phosphide. If the bond length between the aromatic ring and the carbon atom of the carbonyl group (about 1.5 Å) is compared with interatomic distances Ni–P in $Ni_{12}P_5$ and Ni_2P : 2.21–2.59 Å and 2.20 Å, respectively [51], we can conclude that the position of $P^{\delta-}$ would match, approximately, with the center of the aromatic ring. This situation would produce strong electrostatic repulsion between them, moving away the phenyl group from the catalyst surface. As a consequence, a chemoselective hydrogenation of the carbonyl group is produced.

On the other hand, the phosphorus atoms that surround the nickel atoms would produce a diluting effect on the nickel assembly, decreasing the hydrogenation capacity. This would explain why the conversion value is about 30%.

4. Conclusions

In this work, nickel phosphide NPs were obtained by thermal decomposition of a nickel organometallic salt at low temperature. These NPs were monodisperse and their average diameter was 10 nm. Different characterization techniques allowed us to identify these phosphides as a mixture of $Ni_{12}P_5$ and Ni_2P , where each NP is monophasic.

These NPs, supported on mesoporous SiO₂, were used in the catalytic hydrogenation of acetophenone. The catalyst showed hydrogenation capacity and high chemoselectivity to 1-phenylethanol. To our knowledge this is the first time that this type of result has been reported.

We attributed the preferential hydrogenation of the carbonyl group to a combination of the following effects.

- The P and Ni surface atoms have negative and positive charge densities respectively, because P atoms have higher electronegativity than Ni atoms. As a consequence, $Ni^{\delta+}$ can attract the oxygen atom of the carbonyl group.
- The special geometry of the Ni–P sites on the surface of the NPs allows an adequate matching, to produce a strong

electrostatic repulsion of the phenyl group from the surface catalyst.

It should be pointed out that the nickel phosphides have a very wide range of compositions from Ni_3P to NiP_3 . Among them there are great structural differences, producing very diverse catalytic sites. Therefore, we guess that there could be many different types of molecules, with more than one functional group, on which chemoselectivity hydrogenation could take place. As a consequence of these results, we can infer that the great versatility of these phases would justify new studies with different compositions and substrates.

Acknowledgments

This work was supported by Universidad Nacional de La Plata (Projects X633 and X710). The authors are grateful to María Cecilia Moreno, CICPBA translator, for checking the English version.

ORCID iDs

Virginia Vetere  <https://orcid.org/0000-0002-3400-2341>

References

- [1] Fu W, Zhang L, Wu D, Yu Q, Tang T and Tang T 2016 Mesoporous zeolite ZSM-5 supported Ni_2P catalysts with high activity in the hydrogenation of phenanthrene and 4,6-dimethyldibenzothiophene *Ind. Eng. Chem. Res.* **55** 7085–95
- [2] Berenguer A, Sankaranarayanan T M, Gómez G, Moreno I, Coronado J M, Pizarro P and Serrano D P 2016 Evaluation of transition metal phosphides supported on ordered mesoporous materials as catalysts for phenol hydrodeoxygenation *Green Chem.* **18** 1938–51
- [3] Wang X Q, Clark P and Oyama S T 2002 Synthesis, characterization, and hydrotreating activity of several iron group transition metal phosphides *J. Catal.* **208** 321–31
- [4] Shu Y Y and Oyama S T 2005 A new type of nonsulfide hydrotreating catalyst: nickel phosphide on carbon *Chem. Commun.* **9** 1143–5
- [5] Lee Y K and Oyama S T 2006 Bifunctional nature of a SiO_2 -supported Ni_2P catalyst for hydrotreating: EXAFS and FTIR studies *J. Catal.* **239** 376–89
- [6] Oyama S T, Gott T, Zhao H and Lee Y K 2009 Transition metal phosphide hydroprocessing catalysts: a review *Catal. Today* **143** 94–107
- [7] Oyama S T 2003 Novel catalysts for advanced hydroprocessing: transition metal phosphides *J. Catal.* **216** 343–52
- [8] Huang T, Shi W, Xu J and Fan Y 2017 A strategy for preparing highly dispersed Ni_2P /functionalized CMK-3 catalysts with superior hydrodesulfurization performance *Catal. Commun.* **93** 25–8
- [9] Gonçalves V O O, de Souza P M, Teixeira da Silva V, Noronha F B and Richard F 2017 Kinetics of the hydrodeoxygenation of cresol isomers over $\text{Ni}_2\text{P}/\text{SiO}_2$: proposals of nature of deoxygenation active sites based on an experimental study *Appl. Catal. B. Environ.* **205** 357–67
- [10] Li W, Dhandapani B and Oyama S T 1998 Molybdenum phosphide: a novel catalyst for hydrodenitrogenation *Chem. Lett.* **27** 207–8
- [11] Zhao S, Zhang Z, Zhu K and Chen J 2017 Hydroconversion of methyl laurate on bifunctional $\text{Ni}_2\text{P}/\text{AlMCM-41}$ catalyst prepared via *in situ* phosphorization using triphenylphosphine *Appl. Surf. Sci.* **404** 388–97
- [12] Senevirathne K, Burns A W, Russell M E and Brock S L 2007 Synthesis and characterization of discrete nickel phosphide nanoparticles: effect of surface ligation chemistry on catalytic hydrodesulfurization of thiophene *Adv. Funct. Mater.* **17** 3933–9
- [13] Chen Y, She H, Luo X, Yue G-H and Peng D-L 2009 Solution-phase synthesis of nickel phosphide single-crystalline nanowires *J. Cryst. Growth* **311** 1229–33
- [14] Park J, Koo B, Yoon K Y, Hwang Y, Kang M, Park J-G and Hyeon T 2005 Generalized synthesis of metal phosphide nanorods via thermal decomposition of continuously delivered metal-phosphine complexes using a syringe pump *J. Am. Chem. Soc.* **127** 8433–40
- [15] Santhana Krishnan P, Ramya R, Umasankar S and Shanthy K 2017 Promotional effect of Ni_2P on mixed and separated phase $\text{MoS}_2/\text{Al-SBA-15}$ (10) catalyst for hydrodenitrogenation of ortho-Propylaniline *Micropor. Mesopor. Mat.* **242** 208–20
- [16] Wang H, Shu Y, Zheng M and Zhang T 2008 Selective hydrogenation of cinnamaldehyde to hydrocinnamaldehyde over SiO_2 supported nickel phosphide catalysts *Catal. Lett.* **124** 219–25
- [17] Mohr C and Claus P 2001 Hydrogenation properties of supported nanosized gold particles *Sci. Prog.* **84** 311–34
- [18] Bergault I, Fouilloux P, Joly-Vuillemin C and Delmas H 1998 Kinetics and intraparticle diffusion modelling of a complex multistep reaction: hydrogenation of acetophenone over a rhodium catalyst *J. Catal.* **175** 328
- [19] Bergault I, Joly-Vuillemin C, Fouilloux P and Delmas H 1999 Modeling of acetophenone hydrogenation over a Rh/C catalyst in a slurry airlift reactor *Catal. Today* **48** 161–74
- [20] Chen C S, Chen H W and Cheng W H 2003 Study of selective hydrogenation of acetophenone on Pt/SiO_2 *Appl. Catal. A* **248** 117–28
- [21] Santori G F, Moglioni A G, Vetere V, Moltrasio Iglesias G Y, Casella M L and Ferretti O A 2004 Hydrogenation of aromatic ketones with Pt- and Sn-modified Pt catalysts *Appl. Catal. A* **269** 215–23
- [22] Cervený L, Dobrovolná Z, Belohlav Z and Kluson P 1996 Catalytic hydrogenation of acetophenone over ruthenium catalysts *Collect. Czech. Chem. Commun.* **61** 764
- [23] Kluson P and Cervený L 1996 Hydrogenation of substituted aromatic compounds over a ruthenium catalyst *J. Mol. Catal. A* **108** 107–12
- [24] Wismeyer A A, Kieboom A P G and van Bekkum H 1985 Improved activity and selectivity in carbon-oxygen double bond hydrogenation with Ru/TiO_2 *React. Kinet. Catal. Lett.* **29** 311–6
- [25] Drelinkiewicz A, Waksmundzka A, Makowski W, Sobczak J W, Król A and Zięba A 2004 Acetophenone hydrogenation on polymer-palladium catalysts. The effect of polymer matrix *Catal. Lett.* **94** 143–56
- [26] Aramendia M A, Borau V, Gomez J F, Herrera A, Jimenez C and Marinas J M 1993 Reduction of acetophenones over Pd/AlPO_4 catalysts. linear free energy relationship (LFER) *J. Catal.* **140** 335–43
- [27] Aramendia M A, Borau V, Jimenez C, Marinas J M, Sempere M E and Urbano P 1988 Reduction of acetophenone with palladium catalysts by hydrogen transfer and with molecular hydrogen *Appl. Catal.* **43** 41–55
- [28] Tundo P, Zinovyev S and Perosa A 2000 Multiphase catalytic hydrogenation of *p*-chloroacetophenone and acetophenone.

- A kinetic study of the reaction selectivity toward the reduction of different functional groups *J. Catal.* **196** 330–8
- [29] Ishihara A, Hashimoto T and Nasu H 2012 Large mesopore generation in an amorphous silica-alumina by controlling the pore size with the gel skeletal reinforcement and its application to catalytic cracking *Catalysts* **2** 368–85
- [30] Provencher S W 1982 A constrained regularization method for inverting data represented by linear algebraic or integral equations *Comput. Phys. Commun.* **27** 213–27
- [31] Xu R 2002 *Particle Characterization: Light Scattering Methods* (Dordrecht: Kluwer Academic) pp 56–110
- [32] Granqvist C G and Buhrman R A 1976 Ultrafine metal particles *J. Appl. Phys.* **47** 2200–19
- [33] Tan Y *et al* 2014 Optimal synthesis and magnetic properties of size-controlled nickel phosphide nanoparticles *J. Alloy. Compd* **605** 230–6
- [34] Zeppenfeld K and Jeitschko W 1993 Magnetic behaviour of Ni_3P , Ni_2P , NiP_3 and the series $\text{Ln}_2\text{Ni}_{12}\text{P}_7$ ($\text{Ln} = \text{Pr}, \text{Nd}, \text{Sm}, \text{Gd}, \text{Lu}$) *J. Phys. Chem. Solids* **54** 1527–31
- [35] Zheng X, Yuan S, Tian Z, Yin S, He J, Liu K and Liu L 2009 Nickel/nickel phosphide core-shell structured nanoparticles: synthesis, chemical, and magnetic architecture *Chem. Mater.* **21** 4839–45
- [36] Brock S L and Senevirathne K 2008 Recent developments in synthetic approaches to transition metal phosphide nanoparticles for magnetic and catalytic applications *J. Solid State Chem.* **181** 1552–9
- [37] LaGrow A P *et al* 2012 Synthesis, alignment, and magnetic properties of monodisperse nickel nanocubes *J. Am. Chem. Soc.* **134** 855–8
- [38] Carencio S, Boissière C, Nicole L, Sanchez C, Le Floch P and Mézailles N 2010 Controlled design of size-tunable monodisperse nickel nanoparticles *Chem. Mater.* **22** 1340–9
- [39] Carencio S, Le Goff X F, Shi J, Roiban L, Ersen O, Boissière C, Sanchez C and Mézailles N 2011 Magnetic core-shell nanoparticles from nanoscale-induced phase segregation *Chem. Mater.* **23** 2270–7
- [40] Zafiropoulou I, Papagelis K, Boukos N, Siokou A, Niarchos D and Tzitzios V 2010 Chemical synthesis and self-assembly of hollow Ni/Ni₂P hybrid nanospheres *J. Phys. Chem. C* **114** 7582–5
- [41] Wang J, Johnston-Peck A C and Tracy J B 2009 Nickel phosphide nanoparticles with hollow, solid, and amorphous structures *Chem. Mater.* **21** 4462–7
- [42] Savithra G H L, Muthuswamy E, Bowker R H, Carrillo B A, Bussell M E and Brock S L 2013 Rational design of nickel phosphide hydrosulfurization catalysts: controlling particle size and preventing sintering *Chem. Mater.* **25** 825–33
- [43] Li D, Senevirathne K, Aquilina L and Brock S L 2015 Effect of synthetic levers on nickel phosphide nanoparticle formation: Ni_5P_4 and NiP_2 *Inorg. Chem.* **54** 7968–75
- [44] Carencio S, Labouille S, Bouchonnet S, Boissière C, Le Goff X-F, Sanchez C and Mézailles N 2012 Revisiting the molecular roots of a ubiquitously successful synthesis: Nickel(0) nanoparticles by reduction of [Ni(acetylacetonate) 2] *Chem. Eur. J.* **18** 14165–73
- [45] Molina R and Poncelet G 1999 α -alumina-supported nickel catalysts prepared with nickel acetylacetonate. II. A study of the thermolysis of the metal precursor *J. Phys. Chem. B* **103** 11290–6
- [46] Colthup N B, Daly L H and Wiberley S E 1990 *Introduction to Infrared and Raman Spectroscopy* 3rd edn (San Diego USA: Academic)
- [47] Zhang L, He R and Gu H-C 2006 Oleic acid coating on the monodisperse magnetite nanoparticles *Appl. Surf. Sci.* **253** 2611–7
- [48] Chen C, Chen H and Cheng W 2003 Study of selective hydrogenation of acetophenone on Pt/SiO₂ *Appl. Catal. A. Gen.* **248** 117–28
- [49] Li K and Wang R 2011 Hydrodeoxygenation of anisole over silica-supported Ni₂P, MoP, and NiMoP catalysts *J. Chem. Energ. Fuel.* **25** 854–63
- [50] Sawhill S J, Layman K A, Van Wyk D R, Engelhardt M H, Wang C and Bussell M E 2005 Thiophene hydrosulfurization over nickel phosphide catalysts: effect of the precursor composition and support *J. Catal.* **231** 300–13
- [51] Jun R, Wang J-G, Li J-F and Li Y-W 2007 Density functional theory study on crystal nickel phosphides *J. Fuel Chem. Technol.* **35** 458–64